$W^{\pm}Z^0$ and $W^{\pm}\gamma$ pair production in νe, pp, and $\bar{p}p$ collisions

R. W. Brown and D. Sahdev
Physics Department, Case Western Reserve University, Cleveland, Ohio 44106

K. O. Mikaelian
Physics Department, Oklahoma State University, Stillwater, Oklahoma 74074

(Received 2 May 1979)

We augment a previous discussion of the production of pairs of gauge bosons with a study of the reactions pp and $\bar{p}p \to WZ^0X$ or $W\gamma X$. As before, these depend upon trilinear boson couplings and the high-energy behavior is controlled by gauge cancellations. In particular, the (hard) photon production is sensitive to the magnetic-moment parameter κ for the W. We also discuss the related neutrino reactions, $\nu e \to WZ^0$ or $W\gamma$, which may be of interest in very-high-energy cosmic-ray physics.

I. INTRODUCTION

The gauge-boson pair production in colliding-proton collisions

$$\left.\begin{matrix} p+p \\ \bar{p}+p \end{matrix}\right\} \to W^+ + W^- + X \tag{1.1}$$

has recently been analyzed.[1] The original idea[2] was that WW pairs might be copiously produced before reaching the energies where gauge-theory cancellations would take effect, but the detailed analysis showed that such cancellations occur close to threshold just as in[3]

$$e^+ + e^- \to W^+ + W^- . \tag{1.2}$$

The boson mass is the only important scale in energy.

The cancellations themselves remain interesting, however, since they are dependent upon the interrelated coupling scheme in the standard Weinberg-Salam model including charmed quarks and trilinear boson couplings. (It must be remarked that we use the Drell-Yan approximation in the hadron-hadron collision.) We thus view reaction (1.1) as a probe of the electromagnetic and the weak interactions of the W and as an important instance in which renormalizability controls the high-energy behavior of the two body reactions (quark-antiquark annihilation in this case).

The parallel role of the quarks and of the electrons in (1.1) and (1.2) is another example of the similarity between colliding electrons and colliding protons in investigating new physics. In spite of this, there are some practical differences which should be mentioned. The W decay does not have to be dug out of the hadronic debris in (1.2) and *single* W production rates are exactly reversed:

$$pp\ (\bar{p}p) \to WX,\ Z^0X \tag{1.3}$$

are about 3 orders of magnitude *larger* than (1.1), but

$$ee \to We\nu,\ Z^0ee \tag{1.4}$$

are 3 orders of magnitude *smaller* than (1.2). A mitigating circumstance is that colliding proton beams with sufficient c.m. energy are only a few years away and the threshold for pair production (1.1) may be within reach in the not-too-distant future.[4] If and when the W and Z^0 are found via (1.3) and their decay signature better understood, it may be possible to test whether they are *gauge* bosons in reactions such as (1.1). The e^+e^- probe (1.2) is cleaner but perhaps farther into the future.

Since the boson mass is the energy scale beyond which weak and electromagnetic amplitudes are comparable, it follows[1] that

$$e^+ + e^- \to Z^0 + Z^0 \tag{1.5}$$

and

$$\left.\begin{matrix} p+p \\ \bar{p}+p \end{matrix}\right\} \to Z^0 + Z^0 + X \tag{1.6}$$

yield roughly the same rates as (1.2) and (1.1), respectively. In the standard model, nothing very complicated is involved in their calculation and no non-Abelian gauge cancellation occurs. Nongauge vertices (trilinear Z^0) could be studied, however.[5]

The mixed pair production reaction

$$\left.\begin{matrix} p+p \\ \bar{p}+p \end{matrix}\right\} \to W^{\pm} + Z^0 + X \tag{1.7}$$

does involve more interesting amplitudes (the trilinear coupling comes back) and should be comparable in cross-section size to (1.1) and (1.6), in accord with our remarks on boson mass scales. The subject of this paper is to augment the analysis of I with a discussion of (1.7)—see Sec. IV—and also of some other "pair probes."

The basic fermion-antifermion annihilation

 © 1979 The American Physical Society

rates appropriate for (1.7) in Drell-Yan approximation are laid out in Sec. II, together with other calculational preliminaries. It is noticed that this is basically the same calculation needed for the neutrino reaction

$$\bar{\nu}_e + e^- \to W^- + Z^0 , \tag{1.8}$$

which is of possible interest in ultrahigh-energy cosmic-ray physics.[6] The cross section is indeed electromagnetic in size and the results are discussed in Sec. III.

An interesting alternative suggested by (1.7) and (1.8) is the replacement of Z^0 by a *hard* photon:

$$\bar{\nu}_e + e^- \to W^- + \gamma , \tag{1.9}$$

$$\left.\begin{matrix} p+p \\ \bar{p}+p \end{matrix}\right\} \to W^{\pm} + \gamma + X . \tag{1.10}$$

Reaction (1.10) is a rather simpler probe of the W electromagnetic interactions (trilinear $WW\gamma$); our analyses in Secs. II–IV include calculations for (1.9) and (1.10). Conclusions and further ideas are presented in Sec. V.

II. FERMION ANNIHILATION INTO $W^{\pm}Z^0$ AND $W^{\pm}\gamma$

In this section we present the differential and total cross sections for the following reactions:

$$f_i + \bar{f}_j \to W^- + Z^0 , \tag{2.1}$$

$$f_i + \bar{f}_j \to W^+ + Z^0 , \tag{2.2}$$

$$f_i + \bar{f}_j \to W^- + \gamma , \tag{2.3}$$

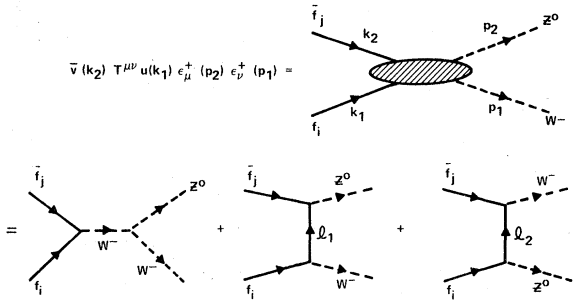

FIG. 1. The lowest-order diagrams for W^-Z^0 production by fermion-antifermion annihilation.

$$f_i + \bar{f}_j \to W^+ + \gamma , \tag{2.4}$$

where f_i stands for one of the fermions ν_e, e, u, d, ..., etc., and $\bar{f}_j$ for the correlated antifermion. The amplitude and Feynman diagrams for reaction (2.1) are shown in Fig. 1, where we also exhibit our notation for the particles involved in that reaction. We follow the same Feynman rules and conventions about coupling constants, etc., as in I. The only new coupling constants needed here are the neutrino neutral-current couplings

$$a_\nu = b_\nu = \tfrac{1}{2} . \tag{2.5}$$

We shall also use the following combination of g_V^i and g_A^i (defined in I):

$$g^i \equiv g_V^i + g_A^i = 2^{1/4} M_Z \sqrt{G_F}\,(a^i + b^i) . \tag{2.6}$$

We have (see Fig. 1)

$$T_{\mu\nu}^{(-)} = iG_{V-A}^{ij}(1+\gamma_5)\left\{ \frac{e_Z}{s-M_W^2}\left[g_{\mu\nu}(\not{p}_2 - \not{p}_1) + \gamma_\nu(2p_1+p_2)_\mu - \gamma_\mu(2p_2+p_1)_\nu \right] - g^j \frac{\gamma_\mu \not{l}_1 \gamma_\nu}{t} - g^i \frac{\gamma_\nu \not{l}_2 \gamma_\mu}{u} \right\} , \tag{2.7}$$

where

$$s=(k_1+k_2)^2=(p_1+p_2)^2, \quad t=l_1^2=(k_1-p_1)^2=(p_2-k_2)^2, \quad u=l_2^2=(k_1-p_2)^2=(p_1-k_2)^2 ,$$
$$s+t+u=M_W^2+M_Z^2 . \tag{2.8}$$

After a rather lengthy calculation, we obtain the following expression for the unpolarized differential cross section:

$$\frac{d\sigma^{(-)}}{dt} = (1+\delta_{j\nu_e})\frac{4\pi\alpha^2}{s^2}\left(\frac{G_{V-A}^{ij}}{e}\right)^2\left\{ \left(\frac{se_Z/e}{s-M_W^2}\right)^2 A(s,t,u) + \frac{2se_Z/e}{s-M_W^2}\left[-\frac{g^j}{e} I(s,t,u) + \frac{g^i}{e} I(s,u,t) \right] \right.$$
$$+ \left(\frac{g^i - g^j}{e}\right)^2 E(s,t,u) + \left(\frac{g^i}{e}\right)^2\left(\frac{ut - M_W^2 M_Z^2}{u^2}\right)$$
$$\left. + 2\left(\frac{g^i g^j}{e^2}\right) s(M_W^2+M_Z^2)/ut + \left(\frac{g^j}{e}\right)^2\left(\frac{ut - M_W^2 M_Z^2}{t^2}\right) \right\} , \tag{2.9}$$

where

$$A(s,t,u) = \left(\frac{ut}{M_W^2 M_Z^2} - 1\right)\left[\frac{1}{4} - \frac{M_W^2+M_Z^2}{2s} + \frac{(M_W^2+M_Z^2)^2 + 8M_W^2 M_Z^2}{4s^2}\right]$$
$$+ \left(\frac{M_W^2+M_Z^2}{M_W^2 M_Z^2}\right)\left[s/2 - M_W^2 - M_Z^2 + (M_W^2 - M_Z^2)^2/2s\right],$$

$$I(s,t,u)=\frac{1}{4}\left(\frac{ut}{M_W^2M_Z^2}-1\right)[1-(M_W^2+M_Z^2)/s-4M_W^2M_Z^2/st]+\left(\frac{M_W^2+M_Z^2}{2M_W^2M_Z^2}\right)[s-M_W^2-M_Z^2+2M_W^2M_Z^2/t],$$

$$E(s,t,u)=\frac{1}{4}\left(\frac{ut}{M_W^2M_Z^2}-1\right)+\frac{1}{2}\frac{s(M_W^2+M_Z^2)}{M_W^2M_Z^2}. \tag{2.10}$$

By setting $M_Z=M_W$, $A(s,t,u)$ and $I(s,t,u)$ can be checked against corresponding terms for $f_i+\bar{f}_i\to W^++W^-$ given in I.

Integrating over t we obtain the total cross section

$$\sigma^{(-)}=\int_{t_{\min}}^{t_{\max}}\frac{d\sigma^{(-)}}{dt}\,dt \tag{2.11}$$

with the limits given by

$$t_{\max,\min}=\tfrac{1}{2}(M_W^2+M_Z^2-s)\pm\tfrac{1}{2}s\beta, \tag{2.12}$$

where

$$\beta=[(1+M_W^2/s-M_Z^2/s)^2-4M_W^2/s]^{1/2}. \tag{2.13}$$

The integrals entering the total cross section are

$$\int A(s,t,u)dt=\frac{s^3\beta^3}{24M_W^2M_Z^2}[1+10(M_W^2+M_Z^2)/s+(M_W^4+10M_W^2M_Z^2+M_Z^4)/s^2],$$

$$\int I(s,t,u)dt=\int I(s,u,t)dt$$

$$=\frac{s^3\beta}{24M_W^2M_Z^2}[1+9(M_W^2+M_Z^2)/s-(9M_W^4+10M_W^2M_Z^2+9M_Z^4)/s^2$$

$$-(M_W^2+M_Z^2)(M_W^4+10M_W^2M_Z^2+M_Z^4)/s^3]-2(M_W^2+M_Z^2)\left[1+\frac{M_W^2M_Z^2}{s(M_W^2+M_Z^2)}\right]\ln L,$$

$$\int E(s,t,u)dt=\int E(s,u,t)dt=\frac{s^3\beta}{24M_W^2M_Z^2}[1+10(M_W^2+M_Z^2)/s+(M_W^2-M_Z^2)^2/s^2], \tag{2.14}$$

$$\int\frac{(ut-M_W^2M_Z^2)}{u^2}dt=\int\frac{(ut-M_W^2M_Z^2)}{t^2}dt=-2s\beta+2s[1-(M_W^2+M_Z^2)/s]\ln L,$$

$$\int\frac{dt}{ut}=\frac{4\ln L}{s-M_W^2-M_Z^2},$$

where

$$L^2=\frac{t_{\min}}{t_{\max}}=\frac{(1+\beta)^2-(M_W^2-M_Z^2)^2/s^2}{(1-\beta)^2-(M_W^2-M_Z^2)^2/s^2}. \tag{2.15}$$

The arrangement and notation has been chosen so as to facilitate comparison with formulas in I for $M_Z=M_W$.

This completes our discussion of $f_i\bar{f}_j\to W^-Z^0$, and we turn to $f_i\bar{f}_j\to W^-\gamma$. We are interested in the $W^\pm\gamma$ production because it may be sensitive to the magnetic moment of the W boson. To expose this dependence, we consider arbitrary values of the familiar "anomalous" moment parameter κ and use the vertex shown in Fig. 2. The Feynman diagrams are the same as in Fig. 1 with $Z^0\to\gamma$.

We shall omit the calculational details. In fact, the differential cross section can be checked against earlier work[7] where the crossed-channel process $\gamma+f_i\to W^\pm+f_j$ was treated. We obtain

$$\frac{d\sigma^{(-)}}{dt}=(1+\delta_{j\nu_e})\frac{\alpha}{s^2}(G_{V-A}^{ij})^2\left\{\frac{(1+\kappa)^2ut}{2(s-M_W^2)^2}-\frac{2sM_W^2}{(s-M_W^2)^2}+\frac{s}{2M_W^2}\left(Q_i-Q_j+\frac{1+\kappa}{2}\right)^2-\frac{ut(\kappa-1)}{4(s-M_W^2)^2}[(1+\kappa)s/M_W^2-2]\right.$$

$$-\frac{ut(\kappa-1)(Q_i-Q_j)}{2(s-M_W^2)M_W^2}+\frac{1}{(s-M_W^2)}\{Q_j[u(1+\kappa)-2sM_W^2/t]-Q_i[t(1+\kappa)-2sM_W^2/u]\}$$

$$\left.+Q_i^2t/u+2Q_iQ_jsM_W^2/ut+Q_j^2u/t\right\}. \tag{2.16}$$

The total cross section is found by integrating over t with the limits given in Eq. (2.12) after setting $M_Z = 0$:

$$\sigma^{(-)} = (1+\delta_{j\nu_e})\frac{\alpha}{s^2}(G^{ij}_{V-A})^2\Big\{(\kappa+1)^2(s-M_W{}^2)/12 - 2sM_W{}^2/(s-M_W{}^2) + \frac{s(s-M_W{}^2)}{2M_W{}^2}\left(Q_i - Q_j + \frac{1+\kappa}{2}\right)^2$$
$$- (s-M_W{}^2)[(1+\kappa)s/24M_W{}^2 - \tfrac{1}{12}](\kappa-1) - (Q_i-Q_j)(\kappa-1)(s-M_W{}^2)^2/12M_W{}^2$$
$$+ \frac{Q_i-Q_j}{s-M_W{}^2}[(1+\kappa)(s-M_W{}^2)^2/2 - 2sM_W{}^2\ln L']$$
$$+ (Q_i{}^2+Q_j{}^2)(s-M_W{}^2)(\ln L'-1) + 4Q_iQ_j\frac{sM_W{}^2}{s-M_W{}^2}\ln L'\Big\}, \tag{2.17}$$

where

$$L' = (s-M_W{}^2)/m_f{}^2, \tag{2.18}$$

in which m_f = fermion mass. In contrast to I, we have had to keep certain fermion-mass dependence in the total-cross-section integration, particularly in the exchange propagators. That is, $t_{\max}$ and $u_{\max} \to 0^-$ as $s \to \infty$. We shall neglect the quark mass differences in the numerical estimates of Sec. IV.

As in Ref. 7, it is worth pointing out that the above expressions simplify considerably for the case $\kappa = 1$, which is the gauge-theory value. In $W^-\gamma$, $Q_j = Q_i + 1$ and the simplifications are

$$\frac{d\sigma^{(-)}}{dt}(\kappa=1) = (1+\delta_{j\nu_e})\frac{\alpha}{s^2}(G^{ij}_{V-A})^2\left(Q_i + \frac{1}{1+t/u}\right)^2 (u^2+t^2+2sM_W{}^2)/ut \tag{2.19}$$

and

$$\sigma^{(-)}(\kappa=1) = (1+\delta_{j\nu_e})\frac{\alpha}{s}(G^{ij}_{V-A})^2\Big\{[2Q_i(Q_i+1)+1]\Big[(1-M_W{}^2/s)(\ln L'-1) + \frac{2M_W{}^2}{s-M_W{}^2}\ln L'\Big]$$
$$- \tfrac{2}{3}(1-M_W{}^2/s) - \frac{2M_W{}^2}{s-M_W{}^2}\Big\}. \tag{2.20}$$

We now turn to the two charge conjugate reactions $f_j + \bar{f}_i \to W^+ + Z^0(\gamma)$. These are obtained from the expressions for W^-Z^0 and $W^-\gamma$ production by interchange of i and j and by reversing the sign of the amplitude where the Z^0 or γ couples to the W (the first Feynman diagram in Fig. 1). Therefore

$$\frac{d\sigma^{(+)}}{dt} = \frac{d\sigma^{(-)}}{dt}\Big|_{\substack{g^i \to -g^j \\ u \to t}} = \frac{d\sigma^{(-)}}{dt}\Big|_{t=(k_{\bar{f}}-P_{W^+})^2}, \tag{2.21}$$

or, in other words, the differential cross section for W^+ production is given by the same expression as for W^- production if we interpret t to be the square of the 4-momentum transferred from the *antifermion* to the W^+. Clearly, the total cross sections are equal,

$$\sigma^{(+)} = \sigma^{(-)}. \tag{2.22}$$

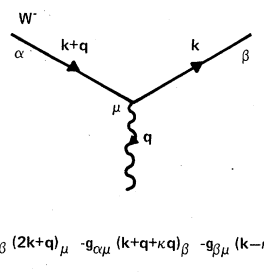

$$-ie\left[g_{\alpha\beta}(2k+q)_\mu - g_{\alpha\mu}(k+q+\kappa q)_\beta - g_{\beta\mu}(k-\kappa q)_\alpha\right]$$

FIG. 2. The electromagnetic vertex for a charged boson with arbitrary magnetic-moment parameter κ.

III. WZ AND $W\gamma$ PRODUCTION BY NEUTRINOS

We shall illustrate the size and the angular dependence of the cross sections derived in the previous sections by considering the specific reactions $\bar{\nu}_e e^- \to W^-Z^0$ and $\bar{\nu}_e e^- \to W^-\gamma$. Again, everything is electromagnetic in magnitude (comparable, say, to $e^+e^- \to \mu^+\mu^-$) when we get to weak-boson-mass c.m. energies, and the features exhibited in this section will be useful in understanding the subsequent quark-antiquark annihilation study.

The actual possibility of detecting the reactions $\bar{\nu}_e e^- \to W^-Z^0$ and $W^-\gamma$ is remote, because truly enormous neutrino energies are required: $E_\nu \gtrsim 10^{16}$ eV for a 100-GeV/c^2 boson mass. This takes us into the realm of cosmic rays where such high-energy neutrinos are indeed expected to be found, albeit in small numbers. Our calculations of the neutrino cross sections are in fact relevant

TABLE I. Values of $x = \sin^2\theta_W$ and the related boson masses considered in the numerical work. θ_W = Weinberg angle, $M_W = M_Z\cos\theta_W = (37.8/\sin\theta_W)$ GeV/c^2.

x	M_W (GeV/c^2)	M_Z (GeV/c^2)
0.15	97.6	106
0.20	84.5	94.5
0.25	75.6	87.3
0.30	69.0	82.5

for project DUMAND (deep underwater muon and neutrino detector),[8] whose purpose is the study of such very-high-energy neutrinos.

We remind the reader that we will use the standard Weinberg-Salam model for all of our numerical calculations. In Table I we give a range of values for $\sin^2\theta_W = x$ embracing results from neutrino physics and the recent polarized-electron experiments,[9] and the values of M_W and M_Z associated with each value of x. We should point out, however, that the reaction $\bar{\nu}_e e^- \to W^-\gamma$ involves no neutral-current couplings—we use x here simply to fix M_W which can be independently varied in this reaction. The same is not true, of course, in the case of $\bar{\nu}_e e^- \to W^- Z^0$, where the relationships between M_W, M_Z and the neutral-current couplings a^i and b^i are crucial to control the high-energy behavior of the total cross section.

We plot the c.m. angular distributions and the total cross sections as a function of $\sqrt{s}$ for each reaction. (Define θ to be the angle between the electron and the W^-.) In Fig. 3 we show $(d\sigma/d\cos\theta)(\bar{\nu}_e e^- \to W^- Z^0)$ at a c.m. energy $\sqrt{s} = 250$ GeV. Two forward-backward peaks are clearly present. The asymmetry between the forward and backward hemispheres increases as we increase x (and the difference between M_Z and M_W), while the total cross section decreases (at this value of $\sqrt{s}$). This last feature, a consequence of the coupling x dependence, is also seen in Fig. 4, where we plot the total cross section as a function of $\sqrt{s}$.

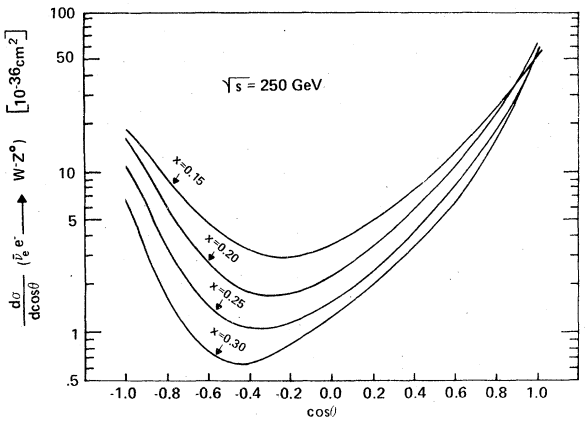

FIG. 3. Differential cross section for $\bar{\nu}_e e^- \to W^- Z^0$. Here θ is the c.m. angle between e^- and W^- (or $\bar{\nu}_e$ and Z_0). The mass range is given in Table I and $\sqrt{s} = 250$ GeV.

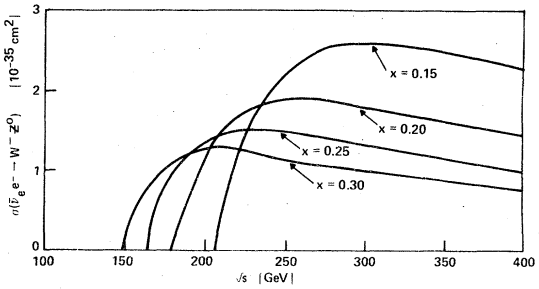

FIG. 4. Total cross sections for $\bar{\nu}_e e^- \to W^- Z^0$. The mass range is given in Table I.

Numerical results for $\bar{\nu} e^- \to W^-\gamma$ will be presented for the popular value of $x = 0.2$ but for different κ, remembering that $\kappa = 1$ corresponds to the gauge-theory em vertex used in I.

In Fig. 5 we plot $d\sigma/d\cos\theta$ for $\bar{\nu}_e e^- \to W^-\gamma$, again at $\sqrt{s} = 250$ GeV. While the curves for $\kappa = -1$ and $\kappa = 0$ are similar, the $\kappa = 1$ curve is strikingly different. This strong κ dependence may be useful in measuring κ in $pp(\bar{p}) \to W^\pm\gamma X$, as discussed in the next section. The $1/u$ behavior seen in Fig. 5 for $\kappa = 1$ is evident also from Eq. (2.19) after setting $Q_i = -1$.

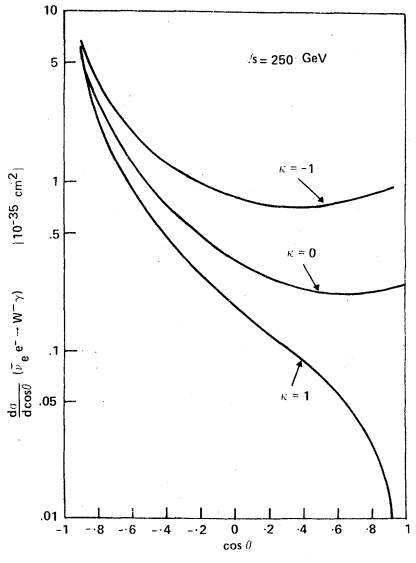

FIG. 5. Differential cross section for $\bar{\nu}_e e^- \to W^-\gamma$. Here θ is the c.m. angle between e^- and W^- (or $\bar{\nu}_e$ and γ), $M_W = 84.5$ GeV/c^2, and $\sqrt{s} = 250$ GeV. κ is the magnetic-moment parameter in the $WW\gamma$ vertex.

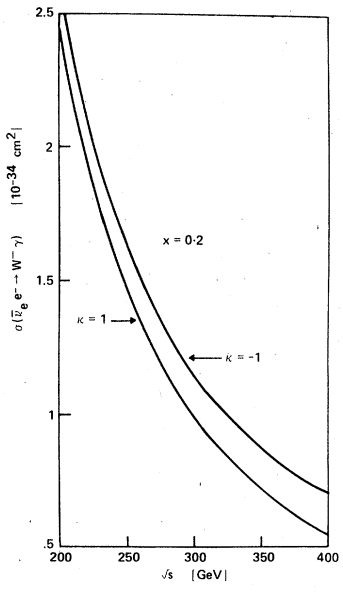

FIG. 6. Total cross sections for $\bar{\nu}_e e^- \to W^-\gamma$. $M_W = 84.5$ GeV/c^2, and κ is the magnetic-moment parameter in the $WW\gamma$ vertex.

In Fig. 6 we plot the total cross section for $\bar{\nu}_e e^- \to W^-\gamma$ as a function of $\sqrt{s}$. The large peaking seen near threshold is due to the soft-photon approach to resonance and requires more careful treatment than we have given it (radiative corrections, resonance width, etc.). But we need only concern ourselves with hard photons. Later, in pp and $\bar{p}p$ collisions where we integrate over the invariant mass of the $W^{\pm}\gamma$ system, we truncate this region (eliminating spuriously large contributions). We also see from Fig. 6 that, in contrast to the angular distribution, the total cross section is not very sensitive to κ.

IV. WZ AND $W\gamma$ PRODUCTION IN pp AND $\bar{p}p$ COLLISIONS

We shall adopt the Drell-Yan model in order to calculate $W^{\pm}Z^0$ and $W^{\pm}\gamma$ production in hadronic collisions. A straightforward adaption of the formulas derived in I gives us the following expression

$$\frac{d\sigma}{d\tau dx_A}(AB \to CDX) = \frac{1}{3x_A}\sum_{i,j}\left[P_i^A(x_A)P_j^B(x_B) + P_j^A(x_A)P_i^B(x_B)\right] \times \sigma_T(q_i\bar{q}_j \to CD), \tag{3.1}$$

where

$$\tau = x_A x_B = Q^2/S,$$
$$Q^2 = (p_C + p_D)^2, \tag{3.2}$$
$$S = (p_A + p_B)^2,$$

and $P_i^A(x_A)$ is the probability of finding a quark q_i in particle A with momentum $x_A P_A$, etc., for which we use the same parametrization as in I. The limits on τ and x_A, over which we later integrate to find the total cross section, are

$$(M_C + M_D)^2/S \leq \tau \leq 1 \text{ and } \tau \leq x_A \leq 1.$$

The quark-antiquark total cross sections $\sigma_T(q_i\bar{q}_j \to CD)$ have been prepared in Sec. II for $CD = W^{\pm}Z^0$ and $W^{\pm}\gamma$. In integrating over τ, we are essentially integrating these cross sections over their c.m. energy $\sqrt{s}$, since $s = \tau S$, where S is the c.m. energy of the pp or $\bar{p}p$ colliding beams.

In this section we fix from the outset $x = 0.2$. To get a feeling for the x (and hence mass) dependence, we refer to the earlier section and also to I, and we point out that the rapid variation of $\sigma(f_i\bar{f}_i \to Z^0Z^0)$ with x, reported in I, does not occur in the two reactions considered here.

In an effort to delineate the κ dependence in $W^{\pm}\gamma$ production, we will give some results for $\kappa = -1$, 0, and +1. In Fig. 7 we plot $(d\sigma/d\tau)(\bar{p}p \to W^{\pm}\gamma X)$ for two values of κ at $\bar{p}p$ c.m. energy $\sqrt{s} = 540$ GeV, a choice motivated by the $\bar{p}p$ project at CERN.[4]

Although the κ dependence of $d\sigma/d\tau$ is seen to be rather weak, the P_t distribution is a different story. To discuss this, consider $u\bar{d} \to W^+\gamma$, which

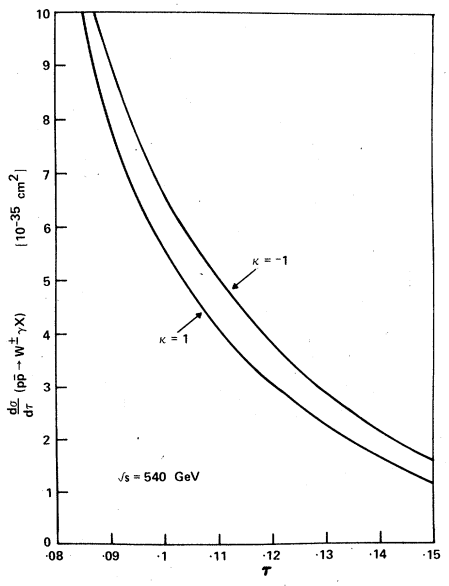

FIG. 7. Invariant-mass distributions for $W^+\gamma$ or $W^-\gamma$ in $\bar{p}p$ collisions.

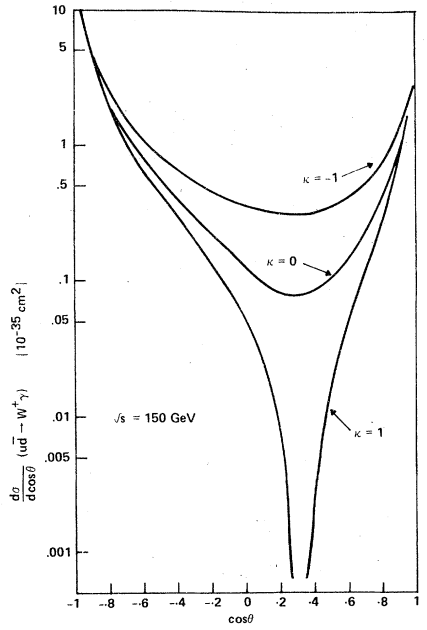

FIG. 8. Angular distribution for $u\bar{d}\to W^+\gamma$ at $\sqrt{s}$ = 150 GeV. A common quark mass of 0.3 GeV/c^2 is assumed and θ is the c.m. angle between u and W^+ (or $\bar{d}$ and γ).

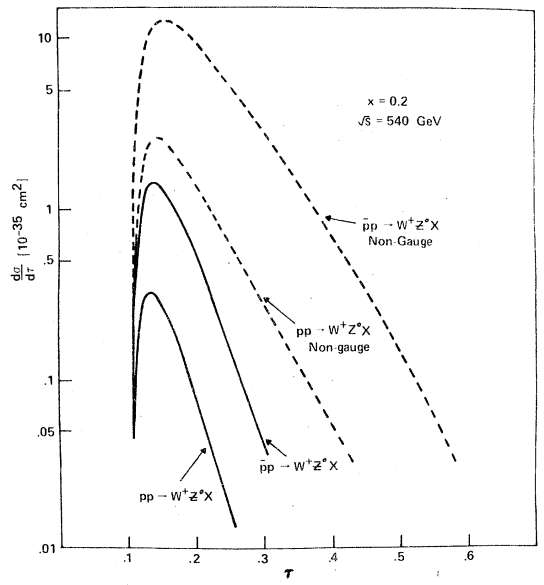

FIG. 9. Invariant-mass distributions for W^+Z^0 in pp and $\bar{p}p$ collisions for $x=0.2$. The two continuous curves correspond to the Weinberg-Salam model and the broken lines correspond to a nongauge theory result with no trilinear boson coupling.

is the quark-antiquark reaction of central importance. The c.m. angular distribution $(d\sigma/d\cos\theta)\times(u\bar{d}\to W^+\gamma)$, where θ is the angle between $\bar{d}$ and W^+, is plotted in Fig. 8 for $\sqrt{s}=150$ GeV (corresponding to $\tau=0.077$ if $\sqrt{s}=540$ GeV). We see that unless $\kappa=1$, the $WW\gamma$ vertex tends to dominate, flattening the angular distributions. As in the neutrino reaction illustrated earlier in Fig. 5, isotropy gives way to more and more forward-backward peaking as the Weinberg-Salam cancellation is approached. Therefore we expect more large-angle or large-transverse-momenta production, particularly for $\bar{p}p$, where the valence quark c.m. frame is closer to the overall c.m. frame the farther we are away from $\kappa=1$.

More mention should be made of the comparison of Figs. 5 and 8. The highly asymmetric distribution $(d\sigma/d\cos\theta)(\bar{\nu}_e e^-\to W^-\gamma)$ is actually due to the electron charge having $Q_e=-1$ [see Eq. (2.19)]. For $u\bar{d}\to W^+\gamma$, $Q_t=-\frac{1}{3}$ and the symmetry is restored. All of this is simply a reflection of the fact that for $\bar{\nu}_e e^-\to W^-\gamma$ the t-channel diagram (corresponding to the second Feynman diagram in Fig. 1 with Z^0 replaced by γ) is not present, while for $u\bar{d}\to W^+\gamma$ both t-channel and u-channel diagrams contribute. The presence of both forward and backward peaking depends upon the fermion charges; whether any peaking is prominant depends upon the κ value.

The divergence of $(d\sigma/d\tau)(\bar{p}p\to W^\pm\gamma X)$ for very small τ is the aforesaid reflection of the infrared resonance region discussed in Sec. III. As we have already indicated, we make a cut to leave out the small τ region (hard photons must be present) in the final integrals needed to get the total cross section. The cut corresponds to $\tau_{\min}=1.1M_W^2/S$. The shapes of $(d\sigma/d\tau)(pp\to W^+\gamma X)$ are similar and have not been plotted.

In Fig. 9 we plot $(d\sigma/d\tau)(pp\to W^\pm Z^0X)$ and $(d\sigma/d\tau)(pp\to W^+Z^0X)$ for $x=0.2$. As an illustration of how the gauge-theory cancellations work, we exhibit in the same figure the result of dropping the trilinear coupling, i.e., dropping the first Feynman diagram in Fig. 1. The shape of the curve does not change much but the whole curve is elevated by a large factor, especially at larger τ values, and the resulting cross section is substantially increased. A similar example is discussed in I, where the effect is shown for a fermion-antifermion cross section $(e^+e^-\to W^+W^-)$.

In Figs. 10 and 11 we plot total production cross sections for all of the boson-pair combinations of I and this paper: W^+W^-, $W^\pm Z^0$, Z^0Z^0, and $W^\pm\gamma$. Though the actual numbers may vary if one uses different quark distribution functions, the relative magnitudes should remain the same to a very good approximation. In the $W^-\gamma$ channel, recall that there is a τ cut made ($\tau_{\min}=1.1M_W^2/S$), but the rates are not too sensitive to this truncation. Of

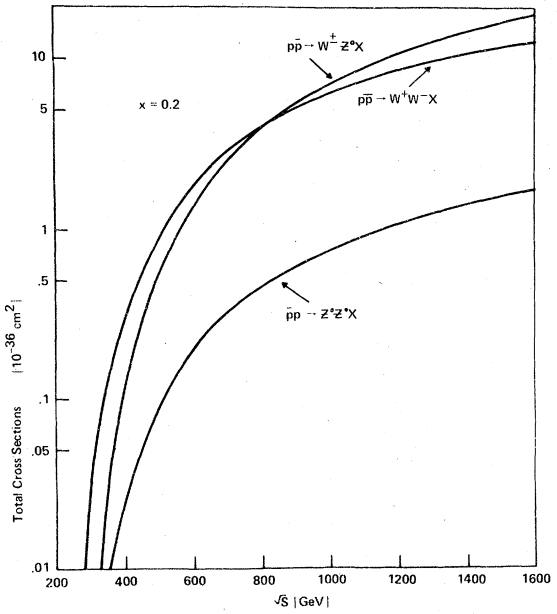

FIG. 10. Total cross sections for the production of boson pairs W^+W^-, $W^{\pm}Z^0$, and Z^0Z^0 in $\bar{p}p$ experiments. Here $x = 0.2$.

course, no such cut is necessary for the $W^{\pm}Z$ channel, where $\tau_{\min} = (M_W + M_Z)^2/S$.

Finally, we turn to pp reactions. In Fig. 12 we plot curves analogous to those in Fig. 10. The difference here between W^+Z^0 and W^-Z^0 is due not to any difference in the basic $q\bar{q} \to W^{\pm}Z^0$ cross sections [see Eq. (2.22)] but rather to the different quark and antiquark content in a proton. The same applies to $W^{\pm}\gamma$, which is plotted in Fig. 11.

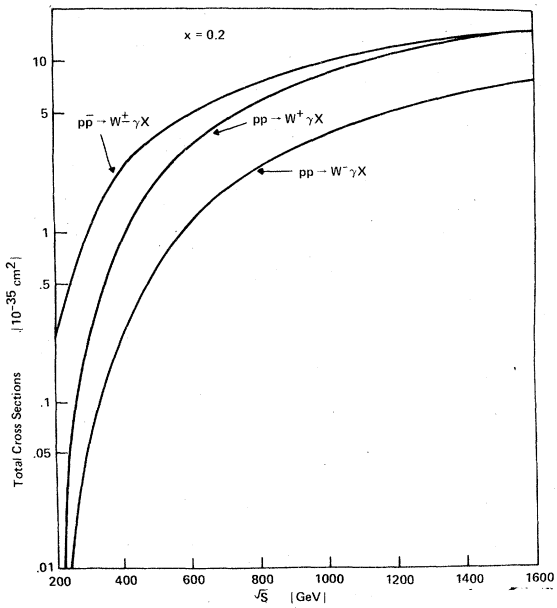

FIG. 11. Total cross sections for $W^{\pm}\gamma$ production in pp and $\bar{p}p$ collisions. Here $x = 0.2$ and $\kappa = 1$.

Clearly, W^+ emission is favored in pp collisions, simply because there are more u quarks. However, everything is down compared to $\bar{p}p$ collisions, an effect due to the presence of valence antiquarks in $\bar{p}$.

V. DISCUSSION

The main thrust of this paper is to detail ways in which proton experiments can show that the weak bosons are actually *gauge* bosons. Presumably they will be found, if they exist and fall in the 100-GeV/c^2 mass range, via reaction (1.3). What we learn there about their decay can then be put to use in the pair-production search, where the gauge cancellations and trilinear boson couplings come into play. Before summarizing and commenting upon some of our pp and $\bar{p}p$ results, we digress with a discussion concerning the lepton reactions.

Lepton-antilepton annihilation into boson pairs can be unified in thought[10] by looking at the square in Fig. 13(a). The general analogous reactions are

$$e^+ + e^- \to x^0, \tag{5.1a}$$

$$\bar{\nu}_e + e^- \to x^-, \tag{5.1b}$$

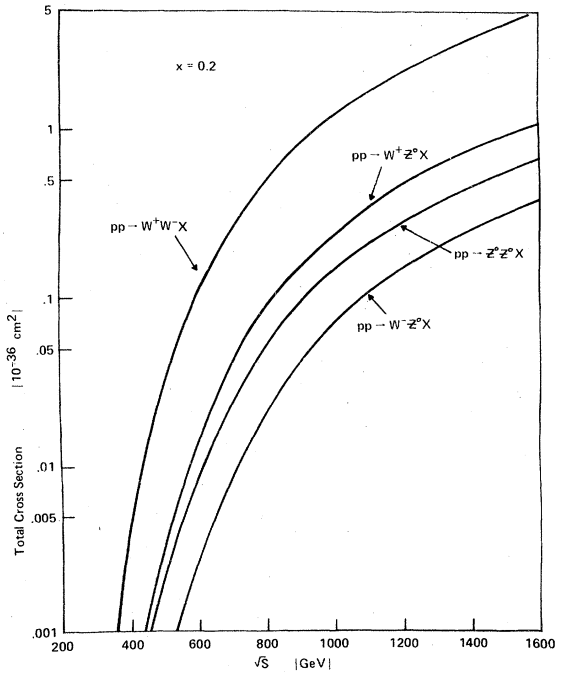

FIG. 12. Total cross sections for the production of boson pairs W^+W^-, W^+Z^0, W^-Z^0, Z^0Z^0 in pp experiments. Here $x = 0.2$.

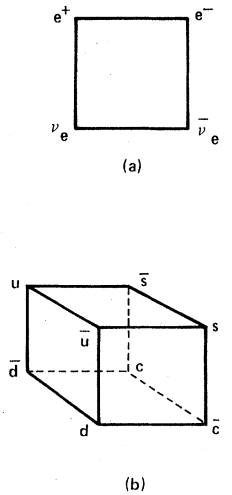

FIG. 13. Adjacent corners of these figures are labeled by fermion pairs which annihilate in two-body reactions. Diagonals are forbidden—nonadjacent corners cannot annihilate in the limit $m_{\text{fermion}} = 0$.

$$\nu_e + e^+ \to x^+, \tag{5.1c}$$

$$\bar{\nu}_e + \nu_e \to x^0 \tag{5.1d}$$

for general x. For example, the much analyzed

$$e^+ + e^- \to Z^0 \tag{5.2}$$

has the analog[11]

$$\bar{\nu}_e + e^- \to W^-. \tag{5.3}$$

[Notice that it is more appropriate to compare (5.2) and (1.2) rather than (1.4) and (1.2) when drawing parallels to (1.1) and (1.3).]

A method for observing (5.3) in a detector such as DUMAND has recently been proposed.[12] The idea is that "direct neutrino" production (charm?) in the atmosphere by ultrahigh-energy primary cosmic rays and subsequent annihilation with atomic electrons in the water detector volume could be seen. Unknown extragalactic sources of $\bar{\nu}_e$ would initiate (5.3) as well.

More generally, such plans may allow us to continue the important business of learning new physics with neutrinos, in spite of the fact that fixed target machine experiments will not see a substantial increase in energy in the near future. Going back to the analogies (5.1), reaction (1.2) suggests the array

$$e^+ + e^- \to W^+ + W^-,\ Z^0 + Z^0, \qquad \text{(1.2) and (1.5)}$$

$$\bar{\nu}_e + e^- \to W^- + Z^0, \tag{1.8}$$

$$\nu_e + e^+ \to W^+ + Z^0, \tag{5.4a}$$

$$\bar{\nu}_e + \nu_e \to W^+ + W^-,\ Z^0 + Z^0, \tag{5.4b}$$

which includes the $\bar{\nu}_e e$ channels we have studied. All of these are the same order in cross-section size (10^{-36}–10^{-35} cm^2 near threshold) and we raise the possibility that $W^- Z^0$ production may be another weak-boson signal in ultrahigh-energy neutrino collisions. The three orders of magnitude difference between the rates for (5.3) and (1.8) can be overcome if the (unknown) fluxes have been underestimated (the pair channel is not confined to a narrow bandwidth).

A similar array can be laid out and perhaps stronger remarks can be made for the other neutrino reaction under scrutiny,

$$\bar{\nu}_e + e^- \to W^- + \gamma. \tag{1.9}$$

This has a somewhat larger cross section and the photon can remain "hard" well below the threshold for (1.8). Comparison of the electron and neutrino cross sections for (1.2), (1.5), (1.8), (1.9), and the electromagnetic standard[13]

$$e^+ + e^- \to \gamma + \gamma \tag{5.5}$$

for which

$$\sigma = \frac{2\pi\alpha^2}{s}\left(\ln\frac{s}{m_e^2} - 1\right), \quad s \gg m_e^2 \tag{5.6}$$

can be found in Fig. 14. For completeness, one should mention that (5.4a) has the same rate as (1.8) and that (5.4b) is a simple version of (1.2) and (1.5).

The parallel nature of e^+e^- and $\bar{\nu}_e e^-$ physics[14,15] means that higher-energy neutrino investigations could lead to the production of resonance states analogous to those in e^+e^- but with different quantum numbers (charge, strangeness, charm),

$$\bar{\nu}_e e^- \to \rho^-,\ K^{*-},\ F^{*-}, \ldots. \tag{5.7}$$

For further discussion see Ref. 15, where the associated Higgs production $\bar{\nu}_e e^- \to W^- H$ is also discussed.

Let us return to more immediate proton physics. The cube in Fig. 13(b) summarizes the quark annihilations possible in weak-boson production. Thus

$$\bar{d}s \not\to \gamma,\ Z^0,\ W^+W^-,\ Z^0Z^0, \tag{5.8}$$

and so forth. This tells us which contributions are present in the Drell-Yan model with the Glashow-Iliopoulos-Maiani (GIM) interactions,[16] given the quark content of the hadron. (By the way, the quark distributions used in our work probably have led us to underestimate the sea contributions, particularly relevant to pp collisions.[17]) The hope of this paper is that these underlying quark interactions, which reflect much gauge theory, can be studied.

Specifically, the size of $d\sigma/d\tau$ reflects the

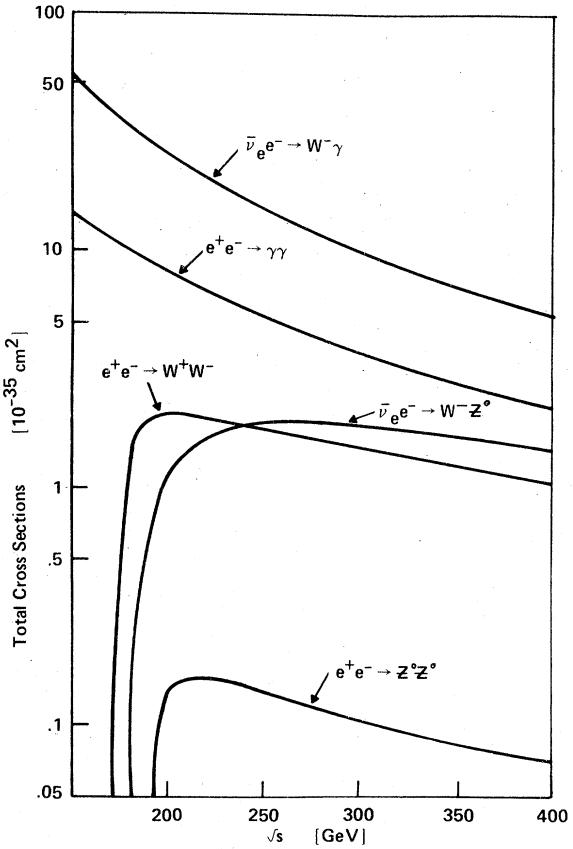

FIG. 14. Total cross sections for lepton annihilation processes for the production of pairs of gauge bosons. Here $\kappa = 1$ and $\chi = 0.2$. The related calculations are described in I, Sec. III, and Ref. 13.

gauge cancellations in $W^{\pm}Z^0$ production. To see this, we removed the trilinear boson coupling in an effort to consider an alternative. The τ distributions increased by roughly an order of magnitude, but in contrast to the e^+e^- Fig. 8 of I, *they do not change in shape*. This would be true for W^+W^- production as well, and is a result of the limited quark phase space at a given S. If the trilinear boson diagram dominated, we would have in addition less peaking along the beam. The c.m. angle isotropy for the $\kappa \neq 1$ $W\gamma$ case would appear here as well.

We should discuss the boson angular distributions a little more. The small angle peaking in $u\bar{d} \to W^+Z^0$, $\bar{u}d \to W^-Z^0$ carries rather directly over to the $\bar{p}p$ frame. In both $\bar{p}p$ and pp, bosons will be found in forward-backward cones around the beam. The cones will be wider for pp than for $\bar{p}p$ in view of the valence-sea x distributions, but some *small* asymmetry (reversed for $W^+ \leftrightarrow W^-$) is present for $\bar{p}p$, since $\langle x \rangle_d \neq \langle x_u \rangle$ and since the quark angular distribution is not perfectly symmetric. Of course, pp leads to exact symmetry. We note then that pp collisions will produce bosons with larger transverse momenta and at times in the same hemisphere.

We have not, however, made a detailed study of boson distributions, let alone the all-important decay spectrum. Some idea of what to expect can be found by coupling the above remarks to the careful single-W analyses.[18] In addition, work done on $e^+e^- \to W^+W^-$, particularly with reference to jets,[19] is useful for us as well.

Stress has been put on $W^{\pm}\gamma$ production as a probe of the moment parameter κ. Varying κ shows up in interesting fashion in angular distribution effects, especially in $\bar{p}p$. Other non-Abelian gauge features (WWZ^0 vertex, GIM mechanism) do not cloud the issue as they would in a κ-dependence study of W^+W^-. Of course, we never break the fundamental U(1) symmetry.

The other interesting aspect of $W^{\pm}\gamma$ production is its larger asymptotic cross section and lower threshold. The threshold is not M_W^2, of course, since we want to see the photon and we need to justify the use of the Drell-Yan model. A hard photon back-to-back with the W fills the bill. The larger cross section arises from the difference in minimum momentum transfers ($t_{\max}$, as it were) and the resulting logarithm arguments.

The logarithmic enhancement brings up an interesting point: Why not replace the hard photon by a hard gluon (jet)? It appears that the running coupling constant in quantum chromodynamics (QCD) will be accompanied by a large logarithm and that the cross sections are significant. A hard-gluon trigger may aid the initial W search.[20]

Finally we mention that $Z^0\gamma$ production, while of the same level as $W^{\pm}\gamma$, is like Z^0Z^0 in that it is perhaps uninteresting in its simplicity. This does bring up the possibility that neutrino counting[21] in e^+e^- collisions,

$$e^+e^- \to \gamma\nu\bar{\nu}, \tag{5.9}$$

can be transcribed to proton collisions as can other tests of Yang-Mills couplings.[22]

ACKNOWLEDGMENTS

In connection with part of this work, R.W.B. is grateful for a stay at the Aspen Center for Physics and K.O.M. wishes to thank C. Quigg for his kind hospitality at Fermilab. Support by the National Science Foundation, Grant Nos. PHY-76-12245 and PHY-78-08883 (R.W.B. and D.S.) and Grant No. PHY-78-11607 (K.O.M.) is hereby acknowledged.

[1]R. W. Brown and K. O. Mikaelian, Phys. Rev. D 19, 922 (1979). We refer to this paper as I in the text.
[2]K. O. Mikaelian, in ISABELLE Summer Study Proceedings, Brookhaven, 1975 (unpublished), Vol. II, p. 340.
[3]W. Alles, Ch. Boyer, and A. J. Buras, Nucl. Phys. B119, 125 (1977); O. P. Sushkov, V. V. Flambaum, and I. B. Khriplovich, Yad. Fiz. 20, 1016 (1974) [Sov. J. Nucl. Phys. 20, 537 (1975)]; G. Komen, Nucl. Phys. B84, 323 (1975); F. Blezacker and H. T. Nieh, *ibid*. B124, 511 (1977).
[4]A. Astbury *et al*., CERN Proposal SPSC/78-06, 1978 (unpublished); BNL Report No. 50648, 1977 (unpublished).
[5]K. J. F. Gaemers and G. J. Gounaris, CERN Report No. TH 2548, 1978 (unpublished).
[6]R. W. Brown, D. Sahdev, J. Stroughair, and K. O. Mikaelian, in *Proceedings of DUMAND 1978 Summer Workshop, LaJolla*, edited by A. Roberts (Scripps Institution of Oceanography, La Jolla, California, 1979).
[7]K. O. Mikaelian, Phys. Rev. D 17, 750 (1978).
[8]*Proceedings of the 1976 DUMAND Summer Workshop, Honolulu*, edited by A. Roberts (Fermilab, Batavia, Illinois, 1977).
[9]C. Y. Prescott *et al*., Phys. Lett. 77B, 347 (1978).
[10]These remarks comprised part of a talk by R. W. Brown, 1978 DUMAND Summer Workshop (unpublished).
[11]S. L. Glashow, Phys. Rev. 118, 316 (1960).
[12]V. S. Berezinsky, D. Cline, and D. N. Schramm, Phys. Lett. 78B, 635 (1978).
[13]See, for example, J. D. Bjorken and S. D. Drell, *Relativistic Quantum Mechanics* (McGraw-Hill, New York, 1964), Sec. 7.8.
[14]I. M. Zheleznykh, in *Proceedings of the 1978 DUMAND Workshop, LaJolla*, edited by A. Roberts (Scripps Institution of Oceanography, La Jolla, California, 1979).
[15]K. O. Mikaelian and I. M. Zheleznykh (unpublished).
[16]S. L. Glashow, J. Iliopoulos, and L. Maiani, Phys. Rev. D 2, 1285 (1970).
[17]Following the analysis of D. M. Kaplan *et al*. [Phys. Rev. Lett. 40, 435 (1978)], we have used a sea proportional to $(1/x)(1-x)^{10}$.
[18]C. Quigg, Rev. Mod. Phys. 49, 297 (1977); R. F. Peierls, T. F. Trueman, and L. L. Wang, Phys. Rev. D 16, 1397 (1977).
[19]M. Perrottet, Marseille Report No. 78/P.1019 (unpublished).
[20]QCD effects on the experimental signatures of single-W searches have been considered by F. Halzen and D. M. Scott, Phys. Lett. 78B, 318 (1978).
[21]E. Ma and J. Okada, Phys. Rev. Lett. 41, 287 (1978); K. J. F. Gaemers, R. Gastmans, and F. M. Renard, Phys. Rev. D 19, 1605 (1979).
[22]F. M. Renard, Languedoc Report No. PM/78/11, 1978 (unpublished).